Ultrafast extended x-ray absorption fine structure (EXAFS)—theoretical considerations

Frank L. H. Brown and Kent R. Wilson
Department of Chemistry and Biochemistry, University of California, San Diego, La Jolla, California 92093-0339

Jianshu Cao
Department of Chemistry, Massachusetts Institute of Technology, Cambridge, Massachusetts 02139

(Received 15 April 1999; accepted 13 July 1999)

Inspired by the recent experimental demonstration of ultrafast x-ray absorption spectroscopy, we present a framework for the calculation of extended x-ray absorption fine structure (EXAFS) spectra on the ultrafast (femtosecond to picosecond) time scale. Model calculations for gas phase I_2, evolving under the influence of laser pumping, demonstrate that ultrafast EXAFS has the potential to serve as a direct probe of nuclear dynamics, including time-dependent interatomic separations and relative orientations. The feasibility of ultrafast EXAFS as a viable and useful experimental technique is discussed. © *1999 American Institute of Physics.* [S0021-9606(99)00338-4]

I. INTRODUCTION

Oscillations in the adsorption spectrum to the high energy side of an x-ray adsorption edge were first observed nearly 80 years ago[1,2] and a qualitative understanding of this phenomenon was provided by Kronig shortly thereafter.[3] Since that time, numerous attempts have been made to quantify the effect (see Ref. 4 for a brief history), but the physical picture remains relatively simple and unchanged. A photoelectron ejected by an atom following x-ray adsorption is subject to the influence of both the ionized atom itself and any neighboring atoms. The presence of neighbors gives rise to a perturbation of the photoelectron's quantum state relative to the case of an isolated photoelectron–positive ion pair. This perturbation is responsible for the oscillations described above and the phenomenon has become known as extended x-ray absorption fine structure (EXAFS). The utility of EXAFS as a means to determine molecular geometries is well-known.[5] Experiment and theory complement each other, allowing, in favorable cases, the determination of interatomic separations to an accuracy of greater than one hundredth of an angstrom.[6] Additionally, the universality of the technique across varied sample types (see Ref. 6 for a series of experiments carried out in the gas, liquid, and solid phases) makes EXAFS a broadly useful experimental tool.

The diversity of problems being tackled by the contemporary EXAFS community is impressive,[7] but the technique remains primarily a tool for the study of stationary systems. The exceptions to this rule include various variants of x-ray absorption spectroscopy on the nanosecond,[8] microsecond,[9] and slower[10] time scales. Such experiments have been useful in elucidating chemical kinetics,[11,12] but are much too coarsely grained in time to probe molecular dynamics. The reason behind this lack of ultrafast x-ray experiments is simple: ultrafast x-ray sources have only recently become a reality. With the advent of several emerging techniques[13–20] to generate ultrafast x-ray pulses, however, the prospect of ultrafast EXAFS seems encouraging. Given the recent advances in ultrafast (femtosecond to picosecond) x-ray experiments, both absorption[21] and diffraction,[13,16,17,19,20,22,23] it seems an opportune time to consider both what could potentially be learned from an ultrafast EXAFS experiment and what is required to make such a measurement.

In previous papers from this group[24–26] and others,[27] the theoretical basis for ultrafast x-ray diffraction has been discussed. In this work, we shall focus on x-ray adsorption, specifically, on EXAFS. Much of the analysis presented here is easily extended to include XANES (x-ray absorption near edge structure), including the phenomena of chemical shift (movement of the absorption edge with changes in the oxidation state of the atom). We have chosen to specifically focus on the EXAFS phenomena since there is an abundance of theoretical understanding and available tools to aid in the calculation of reasonably accurate spectra (at least in the static case). As we will utilize these tools in our time-dependent calculations, and the analogous tools are less well developed for the calculation of XANES signals, we will only discuss EXAFS at this time. The extension to XANES should be clear to the reader, although the actual calculations would be more difficult and less reliable.

The utility of ultrafast EXAFS should prove to be wide ranging. Conventional ultrafast experiments rely upon optical radiation to probe dynamics. The advantage of x-ray-based techniques is that x-rays can probe the nuclear positions of a molecule directly (by interacting with core electrons), whereas optical photons excite valence electrons which extend over multiple nuclei. Relating optical measurements to nuclear dynamics requires a certain amount of *a priori* knowledge about the molecular Hamiltonian to enable inversion from the optical spectrum back to a map of nuclear probability density. With x-ray measurements inversion is easier: no *a priori* knowledge is necessary and, in the case of x-ray diffraction. direct inversion is possible (though not necessarily simple) via Fourier transformation. Although the EXAFS signal is not directly invertible, nuclear positions

may be ascertained by fitting calculated spectra to the experimental spectrum using the nuclear positions as fit parameters. Despite the inconvenience associated with nondirect inversion. EXAFS is an appealing technique because it probes locally—the signal will incorporate effects from a few coordination shells around the adsorbing atom, but not long-range interactions. This locality makes EXAFS particularly appealing for the study of systems in disordered condensed phases (e.g., liquids). Chemical reaction dynamics, solid-state dynamics, and protein dynamics are all potential candidates for study by ultrafast EXAFS. For example, the iron atoms in myoglobin provide suitable subjects for the absorption of x-ray radiation. Portions of the protein proximal to the iron atom will reorient when oxygen, carbon monoxide, or other ligands form complexes with or detach from the protein. This movement will translate into modulation of the EXAFS signal. One can imagine ''seeing'' how myoglobin adapts to carry oxygen as the process takes place! Although nanosecond scale diffraction experiments in this vein have been carried out in crystals,[23] the locality of the EXAFS phenomena could potentially allow for the study of such reactions in the more biologically relevant, aqueous state. The idea of performing temporally resolved EXAFS measurements on myoglobin extends back to at least the middle 1980s.[10] Only now is the technology emerging to carry out such studies over the range of time scales relevant to protein dynamics.

For the purpose of concreteness, we include in this paper a model calculation for the EXAFS signal of gaseous I_2 pumped, by an ultrafast light pulse, to an excited electronic state. The coherent quantum dynamics induced by this transition are observed to temporally modulate the EXAFS signal. Although gas phase I_2 is a far cry from a solvated protein, we believe the underlying physics associated with the EXAFS measurement to be identical for these two systems and, indeed, for any dynamic molecular or condensed phase system. The present work may thus be regarded as a computational proof of principle for the technique of ultrafast EXAFS.

The organization of this paper is as follows. Section II presents a simple means of obtaining the time-dependent EXAFS signal by suitably averaging the usual EXAFS formulas. Details of the derivation needed to arrive at this simple result may be found in the Appendix, which is available electronically.[28] In Sec. III this formalism is used to compute the EXAFS signal for gaseous I_2 under the influence of a molecular ''π'' pulse.[29] This particular example has been chosen both for computational ease and to make contact with previous work on ultrafast x-ray diffraction.[26] In Secs. IV and V we discuss these results and conclude, respectively.

II. PRELIMINARIES

Our goal for this section is to extend the usual EXAFS function, $\chi(k)$ (the absorption cross section normalized to the (atom-like) background with energy measured in terms of the photoelectron wave vector, *k,* ejected in the absorption process), to a time-dependent quantity $\boldsymbol{\chi}(k,t)$ with temporal variation resulting from the electronic and nuclear dynamics of the system. Before proceeding, we note that $\chi(k) \equiv \boldsymbol{\chi}(k,t)$ whenever one is dealing with a sample at equilibrium. This equivalence reflects the fact that EXAFS is an ensemble measurement and that, at equilibrium, any temporal variation in one particular absorber will be observed at a later time in another member of the ensemble. In other words, the EXAFS signal from one individual molecule would in fact show time dependence (assuming a fast enough experiment), but when averaged over the ensemble the spectra become stationary. Such averaging is the physical reason behind the Debye–Waller factors[5] which appear in a conventional treatment. Our discussion rests upon the ability to create a nonequilibrium experimental condition such that the entire ensemble (or some significant portion thereof) is acting in unison. Possibilities for achieving such conditions will be discussed in Secs. III and IV. The following formulas assume such experimental conditions exist.

We now present a brief intuitive justification for the formulas needed in our numerical analysis. Although our final expression turns out to be just what one would naively guess, we stress that this result embodies a number of approximations which will not necessarily hold true in all experimental conditions. A more detailed derivation of our equations, with an emphasis on where approximations have been invoked, may be found in the Appendix.[28]

The x-ray absorption cross section for fixed nuclear coordinates $\mathbf{R}$ is given by

$$\sigma_\alpha(\omega,\mathbf{R}) = 4\pi^2\alpha\omega|\langle\varphi_f|\hat{\mathbf{e}}\cdot\hat{\mathbf{r}}|\varphi_c\rangle|^2 n(\omega), \tag{1}$$

where α is the fine structure constant, ω is the x-ray frequency, $\varphi_f(\mathbf{r};\mathbf{R})$ and $\varphi_c(\mathbf{r};\mathbf{R})$ are the wave functions (following and prior to x-ray absorption, respectively) for the electron which absorbs the x-ray in the one electron approximation,[5] $\hat{\mathbf{e}}$ is the polarization vector for the x-ray $\mathbf{E}$-field, and $n(\omega)$ is the density of photoelectron states at energy $\hbar\omega$ above the energy of $\varphi_c(\mathbf{r};\mathbf{R})$. Conventionally, it is the normalized cross section,

$$\chi(k,\mathbf{R}) = \frac{\sigma(\omega)-\sigma_0(\omega)}{\sigma_0(\omega)}, \tag{2}$$

which is considered in the EXAFS literature. Here, the frequency ω is abandoned in favor of the ejected photoelectron wave vector $k \equiv [2m_e(\hbar\omega - E_0)/\hbar^2]^{1/2}$ defined in terms of the electronic mass, m_e, and E_0, the energy of the edge of the absorption spectra. The ''atomic'' cross section, σ_0, is the cross section for a hypothetical experiment without scattering by neighboring atoms.

We claim (see the Appendix[28] for details) that the time-dependent generalization of Eq. (2) is

$$\boldsymbol{\chi}(k,t) = \frac{\Sigma_i \int d\tau \mathcal{N}(k,\tau-t)\langle\zeta_i(\tau,\mathbf{R})|\chi(k,\mathbf{R})|\zeta_i(\tau,\mathbf{R})\rangle}{\int d\tau \mathcal{N}(k,\tau-t)}, \tag{3}$$

where we must now average Eq. (2) over the Born–Oppenheimer nuclear wave functions $\zeta_i(\tau,\mathbf{R})$ for the occupied valence electronic configurations, *i.* Additional averaging over the intensity profile of the measuring pulse, $\mathcal{N}(k,\tau-t)$, and a sum over the occupied valence electronic states are also required. This equation reflects the fact that

the EXAFS phenomenon occurs much faster than molecular motion. Since we expect the absorption of each x-ray photon to depend only upon the instantaneous configuration of the molecule, Eq. (3) makes perfect sense. The averaging we need to perform just reflects the nuclear distribution over the course of an observation. Equation (3) will serve as the basis for the following numerical study and we note that the availability of packages to calculate $\chi(k,\mathbf{R})$[30,31] makes evaluation of Eq. (3) relatively straightforward.

Although Eq. (3) is ''obviously'' the correct generalization of Eq. (2), we emphasize that it is only valid under a set of approximations outlined in the Appendix.[28] We have, for example, completely neglected cross terms between different electronic states in Eq. (3) which would lead to quantum beats in the EXAFS signal. This particular approximation amounts to assuming no correlation between core and valence electrons and may not be a valid assumption for many systems. The phenomenon of quantum beats has been predicted for x-ray diffraction[26] and could similarly manifest itself in EXAFS despite the fact that Eq. (3) precludes such behavior. Caution must be exercised in the application of the intuitive results presented above and we encourage the interested reader to refer to the Appendix[28] for a detailed derivation of Eq. (3). There, we point out where approximations have been invoked so as to allow for generalization of Eq. (3) when experimental results dictate that we consider a more complicated model.

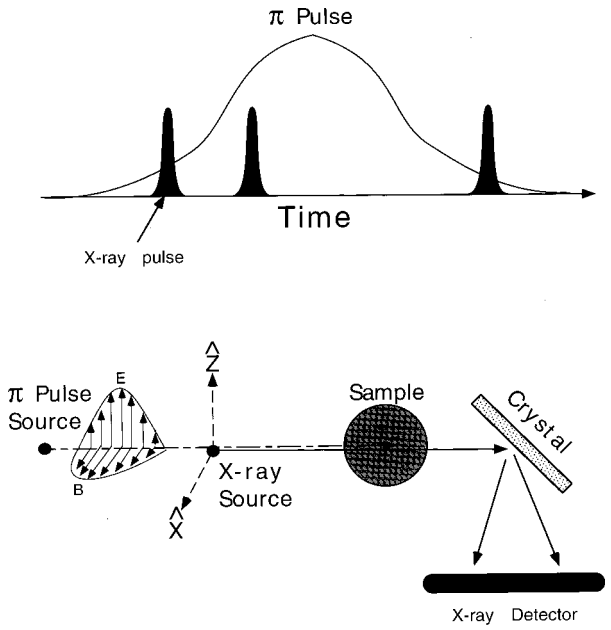

FIG. 1. Schematic diagram of our hypothetical experiment. Top portion: temporal profile for excitation (optical ''π'') pulse and probe (x-ray) pulses. The three probe pulses correspond to the different delay times analyzed in Figs. 2–4. Bottom portion: sketch of the experimental setup showing beam pathways which intersect inside the sample, then an x-ray wavelength dispersing crystal, and finally a detector to monitor absorbence from the x-ray beam versus wavelength. Note that the direction of **E**-field polarization for the optical beam defines the $\hat{\mathbf{Z}}$ direction in our hypothetical experiment.

III. NUMERICAL EXAMPLE

Earlier, we discussed the need for nonequilibrium conditions in order to observe temporal fluctuations in $\boldsymbol{\chi}(k,t)$. Femtosecond optical pulses can initiate such dynamics. As a specific example, we shall consider the time-dependent EXAFS signal for gaseous I_2 subject to a molecular ''π'' pulse.[29,32] The molecular ''π'' pulse excites I_2 from its ground electronic state to an excited electronic state with 99% efficiency, hence the name ''π'' pulse in analogy to the π pulse which inverts population in a two-level system.[33] Excitation to the excited surface initiates coherent motion of the nuclei which can be followed by EXAFS. The hypothetical experiment which we propose is schematically diagramed in Fig. 1. As the (optical) ''π'' pulse excites the molecule. x-ray pulses are fired at the sample to probe the nuclear evolution. As this simple model clearly demonstrates, ultrafast temporal variation in EXAFS can be significant for coherent nuclear dynamics.

Our modeling of the I_2 molecule in the presence of optical excitation, and specifically ''π'' pulse excitation, has been described elsewhere[29,32,34] and we shall limit our discussion of details. We emphasize that the ensuing discussion regarding the interaction between I_2 and light is pertinent only to the creation of the wave function, $|\psi(t)\rangle$, which EXAFS probes. In particular, this discussion is not related to the EXAFS interaction itself, which is described in the preceding section and the Appendix.[28]

The relevant degrees of freedom in this problem are the interatomic distance, r, and rotational angles, (θ,ϕ), of the I_2 molecule as well as the valence electronic state. We assume, for simplicity, an initial condition (prior to interaction with the field) of zero degrees Kelvin for the molecule—i.e., occupation of only the electronic, vibrational, and rotational ground state. The interaction with the field allows for excitation from the ground, X, electronic state to the higher-lying, B, state via a parallel transition ($^3\Pi_{0_u} \leftarrow {}^1\Sigma_{0^+}$ Hund's case c). These surfaces are displaced by 15 769 cm^{-1} relative to one another (see Bardeen *et al.*[34] and references therein). Interaction between I_2 and the electric field is treated semiclasically within the dipole[35] and rotating wave approximation (RWA)[33] approximations. Nuclear vibration on the two surfaces is handled by assuming functional forms of Morse potentials with experimentally determined parameters.[34] Rotational motion is accounted for by expressing the wave function as a sum of spherical harmonics,

$$\psi(t)=\sum_{i}^{B,X}\sum_{J,M} R_{J,i}(r)Y_{J,M}(\theta,\phi), \tag{4}$$

and taking care only to allow field-induced transitions between states with differing electronic states, J values differing by one, and identical M values. Although the field is only capable of inducing $\Delta J=\pm 1$ jumps, the field strengths we are modeling allow for multiple transitions over the course of the simulation, and our final angular distributions reflect an occupation of many different J values. Rovibrational coupling is included by propagating the nuclear wave packets on potential surfaces modified from their Morse form to include the appropriate, J-dependent, centrifugal barriers.

The time-dependent Schrödinger equation for the problem outlined above (full three-dimensional dynamics in the presence of the electric field) is solved numerically to yield

TABLE I. ''π'' pulse parameters.

Parameter	Description	Value
E_0	Field amplitude	20 V/nm
t_0	Temporal center	0
d	Temporal width	100 fs
ω_0	Carrier frequency	19 419 cm^{-1}
c	Chirp rate	5 cm^{-1}/fs

the wave function, $|\psi(t)\rangle$, which is inserted into Eq. (3) to obtain $\boldsymbol{\chi}(k,t)$. We shall assume, for the sake of simplicity, that the x-ray probe pulse is sufficiently fast with respect to nuclear motion to justify the choice

$$\mathcal{N}(\tau-t)=\delta(\tau-t), \tag{5}$$

in Eq. (3) for the x-ray temporal envelope. This choice simplifies our expression for $\boldsymbol{\chi}(k,t)$ to

$$\boldsymbol{\chi}(k,t)=\sum_i \langle\zeta_i(t,r,\theta,\phi)|\chi(k,r,\theta,\phi)|\zeta_i(t,r,\theta,\phi)\rangle, \tag{6}$$

where we have replaced the generic variable set, **R**, with the variables for this particular problem. Extension to a finite pulse duration would simply mean approximating the integrals of Eq. (3) with an appropriate numerical scheme. Computationally, this will be more intensive because of the need to evaluate a number of quantities identical to Eq. (6) for each x-ray probe pulse.

In practice, averaging over the wave function is carried out by choosing a finite discretization to approximate the integrals involved. The values of $\chi(k,r,\theta,\phi)$ on the grid defined by this discretization are calculated using the FEFF software package.[30,36] Repeating the calculation of $\chi(k,r,\theta,\phi)$ for every (r,θ,ϕ) point in this discrete set becomes computationally intensive. By choosing our optical pump pulse to be linearly polarized, however, we insure a level of symmetry (cylindrical about the polarization direction) which enables us to average in two dimensions rather than the full three-dimensional calculation which would have to be performed in the general case. We find that using 100 points in both r ($r\in[2.12,5.29]$ angstrom) and θ (relative angle between ''π'' and x-ray polarizations) is sufficient to obtain convergence for our results.

The precise form chosen for our ''π'' pulse is

$$\mathbf{E}(t)=\hat{\mathbf{Z}}E_0\exp\left[-\frac{(t-t_0)^2}{2d^2}-i\omega_0(t-t_0)-ic\frac{(t-t_0)^2}{2}\right], \tag{7}$$

with parameters as given in Table I. The theory of the molecular ''π'' pulse[29,32] is beyond the scope of this paper, but we point out that this particular choice of parameters leads to better than 99% inversion at time $t=200$ fs. In Figs. 2–4 we present $\boldsymbol{\chi}(k,t)$ for three different time points in the evolution of $|\psi(t)\rangle$ and three different polarization conditions corresponding to x-ray probes polarized both parallel and perpendicular to the optical ''π'' pulse and a polarization averaged measurement. Accompanying each spectrum is a contour plot for the nuclear probability distribution, $\Sigma_i|\zeta_i(t,r,\theta,\phi)|^2$, in the $X-Z$ plane. The changes in this distribution directly lead to the variations in $\boldsymbol{\chi}(k,t)$ and, although the link between distributions and spectra is not completely intuitive, certain connections can be made. Further comments are reserved for the following section.

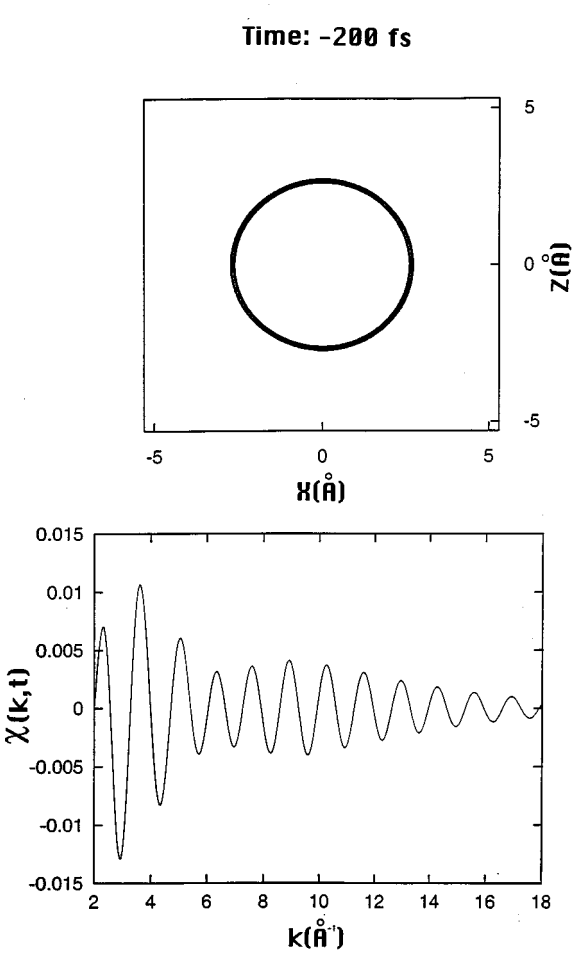

FIG. 2. Top portion: Contour plot (arbitrary units) of the internuclear separation, in angstroms, shown as a probability distribution function in the $X-Z$ plane for I_2 prior to perturbation by the ''π'' pulse. Zero probability is excited to the B state at this time. Since this initial distribution is spherically symmetric, rotation about the Z-axis gives an identical distribution. Bottom portion: EXAFS $\boldsymbol{\chi}(k,t=-200\text{ fs})$ corresponding to the nuclear distribution in the top panel. X-ray polarization averaged, $\hat{\mathbf{Z}}$-polarized, and $\hat{\mathbf{X}}$-polarized EXAFS results are identical due to the symmetry of this configuration.

IV. DISCUSSION

The software package FEFF is an advanced computational tool capable of obtaining near quantitative agreement with experiment for many complicated physical systems.[30] For the modeling of I_2, simpler calculations would have no doubt sufficed, at least to provide a qualitative picture for the phenomena in which we are interested. In the discussion of our results, we shall make use of the relatively crude formula for the K-edge x-ray absorption spectrum,[5,37–39]

$$\chi(k)=-\sum_j (\hat{\mathbf{e}}\cdot\hat{\mathbf{r}}_j)^2\frac{|f_j(\pi,k)|}{kr_j^2}\sin[2kr_j+2\delta_1(k)+\phi_j(k)], \tag{8}$$

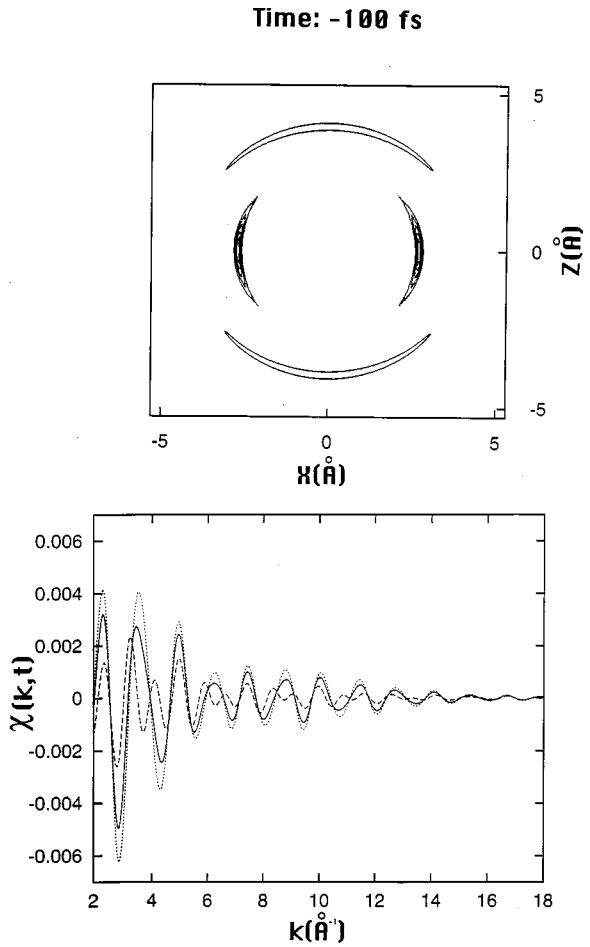

FIG. 3. Similar to Fig. 2 but corresponding to time $t=-100$ fs as defined by Eq. (7). This time corresponds to just over half inversion (56%) to the B state. The three spectra in the bottom panel correspond to x-ray polarization averaged (solid line). $\hat{\mathbf{Z}}$-polarized (dashed line), and $\hat{\mathbf{X}}$-polarized (dotted line) EXAFS measurements. Since the $\hat{\mathbf{Z}}$ polarization of the ''π'' pulse **E**-field defines an axis of symmetry, any x-ray polarization within the $X-Y$ plane will give the same results as the dotted line. Note that the vertical scaling in the bottom panel has changed relative to Fig. 2.

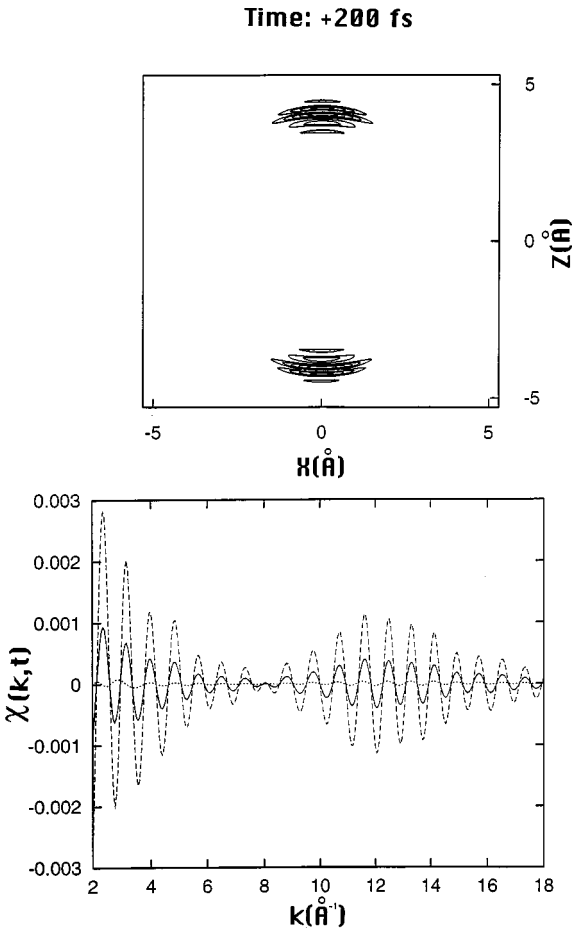

FIG. 4. Similar to Figs. 2 and 3 but corresponding to $t=+200$ fs. Inversion is essentially complete (99%) at this time. Note the large discrepancy between the (strong) $\hat{\mathbf{X}}$-polarized EXAFS and (weak) $\hat{\mathbf{Z}}$-polarized EXAFS signals. This effect is a clear signal that the I_2 molecule has oriented itself predominately along the $\hat{\mathbf{Z}}$-axis.

to explain the qualitative features of our results. In this formula, $\mathbf{r}_j$ is the position vector of the jth scattering atom relative to the absorber, $|f_j(\pi,k)|e^{i\phi_j(k)}$ is the backscattering amplitude from atom j with modulus $|f_j(\pi,k)|$ and argument $\phi_j(k)$, and $\delta_1(k)$ is the $l=1$ partial wave phase shift due to the potential of the absorbing atom. The x-ray polarization is specified by the vector $\hat{\mathbf{e}}$ which is parallel to the x-ray **E**-field.

The essential physics of EXAFS is contained in this equation and we provide a brief justification for the formula here. The EXAFS signal results from a dipole matrix element between the single electron core state, $|\varphi_c\rangle$, and ionized state, $|\varphi_f\rangle$ [see Eqs. (1) and (2)]. Since the core state is tightly localized about the atomic nucleus, it follows that EXAFS is really a probe of photoelectron density (relative to the case without neighboring atoms) at the atomic nucleus following absorption of a photon. The wave function for the photoelectron will consist of a sum of the outgoing spherical wave plus waves scattered back from the neighboring atoms. After subtraction of the background, we expect that the dipole moment will be proportional to a sum over all neighbors of the cross terms between outgoing and backscattered waves. The oscillatory portion of each term in Eq. (8) then embodies the phase accumulated by an electron of wave vector, k, which propagates to and from a neighboring atom. This phase includes a portion from free propagation, $2kr_j$, as well as correction due to phase shifts, $(2\delta_1(k)+\phi_j(k))$.[40] The r_j^{-2} terms stem from the flux of electrons through unit area at a distance r_j removed from the core wave function site. The backscattering amplitude, $|f_j(\pi,k)|$, reflects the square root of the probability that a portion of this flux is redirected back toward the atom from which the electron originated. Although we find it useful to interpret our results in terms of this simple picture, we emphasize that the actual calculations were not performed using Eq. (8). We may think of Eq. (8) as a convenient and simple model upon which to understand the results of our more exact numerical experiment.

We note that the functional form of Eq. (8) is actually quite general given that $|f_j(\pi,k)|$. $\delta_1(k)$, and $\phi_j(k)$ may exhibit arbitrary k dependence. We have verified the validity of Eq. (8) for our system by decomposing the FEFF-generated signal for $t=-200$ fs into amplitude and phase as discussed by Lee *et al.*[5] Substitution of the resultant amplitude and

phase into Eq. (8) yields an EXAFS spectrum indistinguishable from the FEFF $\chi(k,t=-200\,\text{fs})$ of Fig. 2. It will not always be the case that Eq. (8) is in perfect agreement with more detailed calculations (problems will arise in systems for which multiple scattering is important), but we are confident in using the simple formula as a means to discuss our results for this set of simulations.

Given our results for the time-dependent function, $\chi(k,t)$, [Eq. (3)] and our assumed form for the x-ray pulse envelope [Eq. (5)], it is clear that the spectra recorded in Figs. 2–4 directly result from the averaging of $\chi(k,r,\theta,\phi)$ over the internuclear probability distribution at time t. Several features in the spectra are easily explained by reference to Eq. (8) and we shall enumerate these features shortly; however, we first describe the proposed experiment and calculated spectra on purely qualitative grounds to maximize clarity.

Our experiment begins with an ensemble of identically prepared, gas phase, I_2 molecules in the ground electronic, vibrational, and rotational states. The nuclear probability distribution for this ensemble of molecules (or, equivalently, for a single one of the molecules) is a spherical shell with a mean radius corresponding to the equilibrium bond length of the ground state for I_2 (2.67 Å) and a very narrow radial spread corresponding to zero point motion along the internuclear coordinate. This distribution and the corresponding EXAFS signal are found in Fig. 2. The spherically symmetric nature of the probability distribution insures that any polarization direction chosen for the x-rays will provide an equivalent result. We shall take this ''pre ''π'' pulse'' spectra to be the measuring stick against which the other spectra will be compared.

With the introduction of the optical excitation provided by the ''π'' pulse, the symmetry described above is broken. The direction of **E**-field polarization for the ''π'' pulse serves to define a preferred direction in our previously isotropic experiment. We take the direction of this **E**-field to be the $\hat{\mathbf{Z}}$ direction [see Eq. (7) and Fig. 1]. *The optical* **E***-field polarization defines the* $\hat{\mathbf{Z}}$ *direction for us. All following references to polarization direction refer to the polarization of the* **E***-field of the x-ray probe pulse. The* $\hat{\mathbf{X}}$ *and* $\hat{\mathbf{Z}}$ *experiments described below and in the figure captions may thus be thought of as experiments with perpendicular and parallel relative polarizations between the optical and x-ray pulses, respectively.*

The effect of the ''π'' pulse on the nuclear distribution is twofold. First, the average bond length of the I_2 molecule increases as is expected for a transition to an excited electronic state with a less attractive potential surface. Since EXAFS measures the backscattering of photoelectrons off neighbors, the EXAFS signal is expected to decrease and become more oscillatory with such a lengthening of the bond. This effect is clearly observed in Figs. 3 and 4. The second effect of the ''π'' pulse is to align the molecule with the optical field. This alignment results from the selection rules for radiative transitions which specify $\Delta J=\pm 1$ and $\Delta M=0$. As the ''π'' pulse proceeds, the valence electrons jump back and forth between the ground and excited states creating a distribution over many J values, but retaining the initial $M=0$ configuration. This nonisotropic distribution of angular momentum corresponds to a molecule preferentially aligned with the optical field. This alignment is incomplete in Fig. 3, but by Fig. 4 the molecule is clearly predominately $\hat{\mathbf{Z}}$-aligned. Since the ejected photoelectron is preferentially sent off in the direction of x-ray polarization, we expect to see a drastic decrease in EXAFS signal for the $\hat{\mathbf{X}}$-polarized experiment at late times in the ''π'' pulse progression. This effect is most obvious in Fig. 4, where the signal is practically flat for the $\hat{\mathbf{X}}$-polarized experiment and the $\hat{\mathbf{Z}}$-polarized signal is still sizable despite the much inflated bond length.

For clarity, we restate the three basic points made clear in our series of snapshots. These general points will hold true for any ultrafast EXAFS as they are general consequences of the EXAFS phenomena.

(1) X-ray polarization makes a difference. The $(\hat{\mathbf{e}}\cdot\hat{\mathbf{r}}_j)^2$ factor in Eq. (8) makes this clear. Note in particular how the $\hat{\mathbf{Z}}$-polarized, $\hat{\mathbf{X}}$-polarized, and polarization averaged spectra show identical results for the isotropic distribution of $t=-200$, but vastly different results for later times when the symmetry of the I_2 wave function is broken. By performing linearly polarized EXAFS measurements over a range of x-ray polarization directions relative to the optical pump, information about the relative angular distributions of atoms may be obtained. In Fig. 4, for example, the striking difference in signal strength between $\hat{\mathbf{Z}}$- and $\hat{\mathbf{X}}$-polarized EXAFS measurements shows that the I–I bond is predominantly aligned along the direction of the optical ''π'' pulse ($\hat{\mathbf{Z}}$ direction).

(2) Increasing the bond length leads to a sharp decrease in the signal strength. The strongest signal is clearly for the initial configuration. As the ''π'' pulse begins the excitation, the mean bond separation increases and the signal drops. The $1/r^2$ term is responsible for this. Physically, the effect results from the reduced amplitude for the ionized electron to be backscattered by a more distant atom (recall that EXAFS is due to this backscattering effect[5,37]).

(3) The ''wiggles'' show increase in frequency as the bond length increases. This effect comes from the sin term in Eq. (8) and some success has been achieved for determining bond lengths by simple Fourier inversions of equilibrium EXAFS signals.[5] The fact that we are averaging over a distribution of bond lengths and orientations precludes us from quantitatively inverting in such a simple fashion: however, it is possible to qualitatively invert the EXAFS signal as we discuss below.

The simplest means to gain information from stationary EXAFS signals is to consider the modified Fourier transform of $\chi(k)$ as summarized by Lee *et al.*[5] Although one expects this technique to be most successful in interpreting polarization averaged measurements on well-localized distributions, we have applied the technique to our numerically generated spectra with encouraging results. Figures 5–7 present the magnitude of the Fourier transforms for $k^3\chi(k,t)$ corresponding to the $\chi(k,t)$'s of Figs. 2–4. Although it may be tempting to view these curves as radial distribution func-

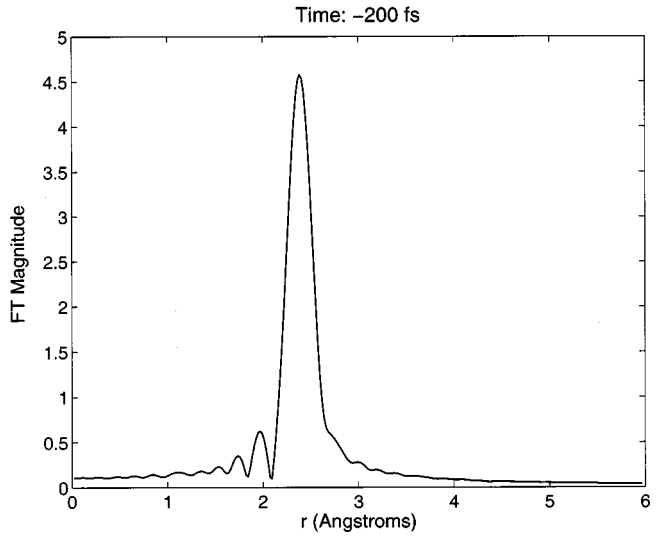

FIG. 5. Magnitude of the Fourier transform for the EXAFS signal in Fig. 2 corresponding to the I_2 molecule prior to arrival of the optical ''π'' pulse. The peak approximately corresponds with the bond length of I_2 (2.67 Å). Note the changes in vertical scale among Figs. 5, 6, and 7.

tions, this interpretation is clearly incorrect, as should be evident through inspection of Eq. (8). First, $|f_j(\pi,k)|$ does not decay exactly as $1/k^2$ (or even very close to this behavior for I_2[6]) and the possibility of strong k dependence in the phase shift terms $[\delta_1(k)$ and $\phi_j(k)]$ would lead one to believe that Fourier transformation has no hope of reproducing nuclear distributions. Fortunately, the phase shifts are often well represented by expansions truncated at linear order in k.[38] When this is the case, the Fourier transformation described above will peak, not where nuclear density is highest,

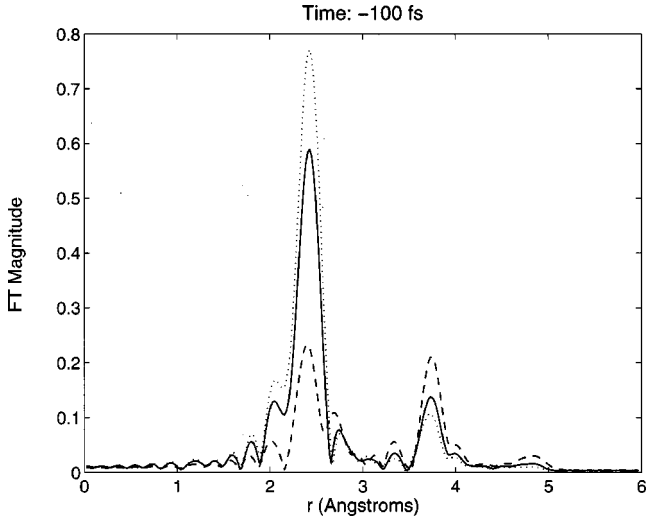

FIG. 6. Magnitude of the Fourier transforms for the EXAFS signals in Fig. 3 corresponding to $t=-100$ fs. The three lines correspond to x-ray polarization averaged (solid line). $\hat{\mathbf{Z}}$-polarized (dashed line), and $\hat{\mathbf{X}}$-polarized (dotted line) EXAFS measurements. The two peaks roughly correspond to the clusters of nuclear distribution observed in the top panel of Fig. 3. The change in relative height of the two peaks as the x-ray polarization is rotated serves as a qualitative indicator that the ''distant'' portion of the distribution is predominately $\hat{\mathbf{Z}}$-aligned and the ''near'' portion lies predominately on and near the $\hat{\mathbf{X}}$–$\hat{\mathbf{Y}}$ plane.

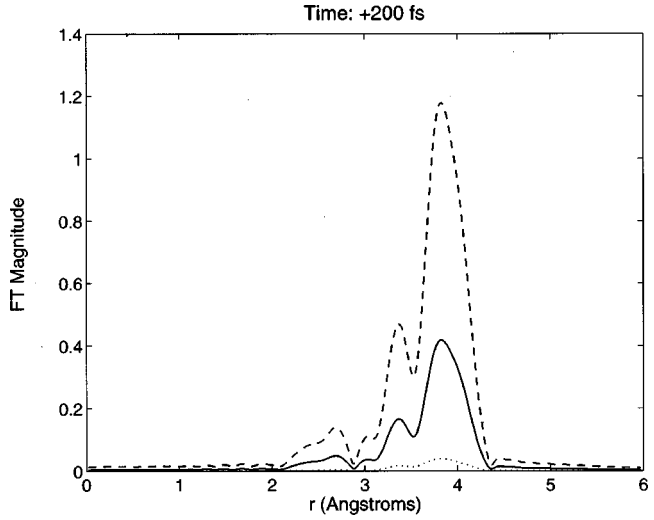

FIG. 7. Similar to Figs. 5 and 6, but with Fourier transforms corresponding to $t=+200$ fs and the signals of Fig. 4.

but offset from this distance by an amount equal to 1/2 of the linear coefficient of the sum of the phase shifts.[38]

We have verified that the argument of the sin term of Eq. (8) shows linear k dependence by decomposing our signals into amplitude and phase as previously discussed and find that our offset is approximately -0.2 Å. The peaks in Figs. 5–7 are thus seen to correspond to the regions of highest nuclear density in the top panels of Figs. 2–4. As the ''π'' pulse is turned on, the ground-state peak (near 2.5 Å but corresponding to 2.7 Å of I_2 separation) decreases in intensity and a new peak grows in at larger r (3.8 Å corresponding to 4.0 Å of I_2 separation), agreeing with the nuclear density plots. Implicit in the above discussion is the fact that phase transferability[5,38] applies between different times in our simulation. This has been verified, explaining why our transforms succeed as well as they do.

It is also possible to infer the approximate angular dependence of the distributions by observing relative peak height changes as x-ray polarization is rotated. In Fig. 6, for example, the $\hat{\mathbf{X}}$-polarized measurement shows a far larger peak near the ground-state equilibrium bond length than does the $\hat{\mathbf{Z}}$-polarized one. We are led to conclude that nuclear density is leaving the equilibrium bond separation along the $\hat{\mathbf{Z}}$-axis. Concurrently, a new peak grows in at 4 Å, predominately $\hat{\mathbf{Z}}$-aligned, in agreement with the nuclear distribution at $t=-100$ fs. Our calculations suggest that it will be relatively easy to follow gross changes in ultrafast physical behavior by simply Fourier transforming the experimental data. We stress that such a transformation will be only a qualitative tool; quantitative inversion will be a much more challenging problem.

The problem of inversion is certainly of prime importance. For standard EXAFS problems, inversion is usually carried out by fitting experimental spectra to models with a number of variable parameters (bond distances, Debye–Waller factors, etc.). The set of parameters yielding the best fit to the data is taken to represent the configuration of the sample being studied. Our time-dependent, fully quantum mechanical, calculation has demonstrated that even a simple

experiment designed to probe molecular dynamics can lead to significant spreading of nuclear wave packets. The diffuse nature of the nuclear probability distribution in such an evolving sample is not amenable to description by a ''time-dependent Debye–Waller'' factor or the like. In practice, ''inversion,'' particularly for more complex systems, will likely have to be carried out by comparing experimental results to simplified calculations (based upon classical or semiclassical molecular dynamics where wave packet spreading is lessened) or by iterative fitting of spectra to model spectra based upon various parametrized functional forms for nuclear distributions. Such procedures will have to be investigated once experimental data become available for analysis.

From a theoretical standpoint, ultrafast time-resolved EXAFS shows promise as a means to follow molecular dynamics, but we point out that our simulations are idealized. To date, ultrafast EXAFS has not been experimentally demonstrated and it is doubtful that the first attempts at such an experiment will conform to our idealized model of infinitely sharp temporal x-ray pulses. Even in an idealized experiment, the variation in the EXAFS signal is a small percentage of the height of the edge of the absorption line. Achieving a good signal-to-noise ratio may prove to be difficult for delocalized atoms distant from one another. Although stationary EXAFS signals can reveal information about localized atoms in the second and further solvation shells, spatial averaging over delocalized wave packets significantly complicates inversion for large separations. As a final note of caution, we return to the approximation [Eq. (5)]. Such an approximation translates, for the I_2 system presented, into x-ray pulse durations on the order of tens to hundreds of femtoseconds. Such x-ray pulse durations have yet to be conclusively demonstrated, although there appear to be no fundamental physical limitations to achieving them with accelerator, plasma, or x-ray laser sources. For a nonzero x-ray pulse length, there will be additional averaging which will tend to ''wash out'' $\boldsymbol{\chi}(k,t)$, making inversion back to $|\psi(t)|^2$ correspondingly more challenging.

V. CONCLUSION

The present work represents an initial theoretical discussion of ultrafast EXAFS. It is a consequence of the disparity in time scales between x-ray coherence and molecular motion that time-resolved EXAFS spectra amount to averages over the well-studied, time-independent $\chi(k)$. Although this averaging may be time consuming in simulations, the scaling of the problem will be linear with the time consumed by a single time-independent $\chi(k)$ calculation. The existence of well-established methods for the computation of $\chi(k)$ has made our calculations of $\boldsymbol{\chi}(k,t)$ relatively simple to implement. Our initial investigation on I_2 has led us to believe that ultrafast EXAFS has potential as a means of following nonequilibrium, coherent molecular dynamics.

The close theoretical connection between $\boldsymbol{\chi}(k,t)$ and the conventional $\chi(k)$ insures that, on a qualitative level, spectra are relatively easy to interpret for sufficiently simple systems. Inversion for more complex, time-dependent systems will be challenging, particularly for diffuse nuclear distributions. It seems likely, though, that qualitative estimates of time-dependent bond lengths may be gained from simple Fourier inversions of $\boldsymbol{\chi}(k,t)$. Similarly, the angular dependence associated with the $(\hat{\mathbf{e}}\cdot\hat{\mathbf{r}}_j)^2$ term of Eq. (8) will serve as a guide to relative orientational dynamics in evolving systems.

Another feature of x-ray absorbence which might prove useful in ultrafast measurements is the chemical shift (altering of the position of an absorption edge resulting from changes in electron density about the central atom). Although our treatment has not included coupling between the absorbing electron and the valence electrons of the molecule, modification to include such effects would be possible by explicitly retaining the valence electron dependence of the core electronic states in Eq. (A10).[28] Such a generalization would, for example, provide a simple picture for modeling the time-dependent chemical shift associated with charge transfer reactions.

With x-ray sources capable of delivering subpicosecond pulses of radiation over a sufficiently broad band of frequencies expected to become available, time-resolved EXAFS can prove to be an important tool in the study of molecular dynamics, solid state dynamics, localized protein dynamics, and related dynamical phenomena. This study indicates that, at least, semiquantitative interpretation of such proposed ultrafast EXAFS experiments should be possible.

ACKNOWLEDGMENTS

We thank Professor John Rehr (University of Washington) and Dr. Ting Guo (UCSD) for helpful discussions.

[1] H. Fricke, Phys. Rev. **16**, 202 (1920).
[2] G. Hertz, Z. Phys. **3**, 19 (1920).
[3] R. Kronig, Z. Phys. **70**, 317 (1931); **75**, 468 (1932); **76**, 468 (1932).
[4] E. A. Stern, in *EXAFS Spectroscopy*, edited by B. K. Teo and D. C. Joy (Plenum, New York, 1981).
[5] P. A. Lee, P. H. Citrin, P. Eisenberger, and M. Kincaid, Rev. Mod. Phys. **53**, 769 (1981).
[6] U. Buontempo, A. Di Cicco, A. Filipponi, M. Nardone, and P. Postorino, J. Chem. Phys. **107**, 5720 (1997).
[7] *Proceedings of the Tenth International Conference on X-ray Absortion Fine Structure* XAPS X, J. Synchrotron Radiation **6**, 121 (1999).
[8] A. Rogalev and J. Goulon, J. Phys. IV **7**, C2-565 (1997).
[9] M. R. Chance, M. D. Wirt, E. M. Scheuring, L. M. Miller, A. Xie, and D. E. Sidelinger, Rev. Sci. Instrum. **64**, 2035 (1993).
[10] D. M. Mills, A. Lewis, A. Harootunian, J. Huang, and B. Smith, Science **223**, 811 (1984).
[11] Y. Inada, H. Hayashi, and S. Funahashi, Rev. Sci. Instrum. **68**, 2973 (1997).
[12] L. X. Chen, M. R. Wasielewski, T. Rajh, P. L. Lee, M. C. Thurnauer, and P. A. Montano, J. Phys. IV **7**, C2-569 (1997).
[13] T. Anderson, I. V. Tomov, and P. M. Rentzepis, J. Chem. Phys. **99**, 869 (1993).
[14] M. M. Murnane, H. C. Kapteyn, M. D. Rosen, and R. W. Falcone, Science **251**, 531 (1991).
[15] R. W. Schoenlein, W. P. Leemans, A. H. Chin, P. Volfbeyn, T. E. Glover, P. Balling, M. Zolotorev, K.-J. Kim, S. Chattopadhyay, and C. V. Shank, Science **274**, 236 (1996).
[16] J. Larsson, P. A. Heimann, A. M. Lindenberg, P. J. Schuck, P. H. Bucksbaum, R. W. Lee, H. A. Padmore, J. S. Wark, and R. W. Falcone, Appl. Phys. A: Mater. Sci. Process. **66**, 587 (1998).
[17] T. Guo, C. Rose-Petruck, R. Jimenez, F. Raksi, J. A. Squier, B. C. Walker, K. R. Wilson, and C. P. J. Barty, Proc. SPIE **3157**, 84 (1997).
[18] W. P. Leemans, R. W. Schoenlein, P. Volfbeyn, A. H. Chin, T. E. Glover, P. Balling, M. Zolotorev, K. J. Kim, S. Chattopadhyay, and C. V. Shank, Phys. Rev. Lett. **77**, 4182 (1996).

[19] C. Rischel, A. Rousse, I. Uschmann, P.-A. Albouy, J.-P. Geindre, P. Audebert, J.-C. Gauthier, E. Forster, J.-L. Martin, and A. Antonetti, Nature (London) **390**, 490 (1997).
[20] C. Rose-Petruck, R. Jimenez, T. Guo, A. Cavalleri, C. W. Siders, F. Raksi, J. A. Squier, B. C. Walker, K. R. Wilson, and C. P. J. Barty, Nature (London) **398**, 310 (1999).
[21] F. Raksi, K. R. Wilson, Z. Jiang, A. Ikhlef, C. Y. Cote, and J.-C. Kieffer, J. Chem. Phys. **104**, 6066 (1996).
[22] *Time Resolved Diffraction*, edited by J. R. Helliwell and P. M. Rentzepis (Clarendon, Oxford, 1997).
[23] V. Srajer, T. Teng, T. Ursby, C. Pradervand, Z. Ren, S. Adachi, W. Schildkamp, D. Bourgeois, M. Wulff and K. Moffat, Science **274**, 1726 (1996).
[24] J. P. Bergsma, M. H. Coladonato, P. M. Edelsten, K. R. Wilson, and D. R. Fredkin, J. Chem. Phys. **84**, 6151 (1986).
[25] M. Ben-Nunn, J. Cao, and K. R. Wilson, J. Phys. Chem. **101**, 8743 (1997).
[26] J. Cao and K. R. Wilson, J. Phys. Chem. **102**, 9523 (1998).
[27] S. H. Lin, C. H. Chao, H. Ma and P. M. Rentzepis, in *Time-Resolved Electron and X-ray Diffraction*, Proceedings of SPIE-Int. Soc. Opt. Eng. **2521**, 258 (1995), edited by P. M. Rentzepis.
[28] See EPAPS Document No. E-JCPSA6-111-003938 for a PDF format appendix of this work. This document may be retrieved via the EPAPS homepage (http://www.aip.org/pubservs/epaps.html) or from ftp.aip.org in the directory /epaps/. See the EPAPS homepage for more information.
[29] J. Cao, C. J. Bardeen, and K. R. Wilson, Phys. Rev. Lett. **80**, 1406 (1998).
[30] S. I. Zabinsky, J. J. Rehr, A. Ankudinov, R. C. Albers, and M. J. Eller, Phys. Rev. B **52**, 2995 (1995); J. Mustre de Leon, J. J. Rehr, S. I. Zabinsky, and R. C. Albers, *ibid.* **44**, 4146 (1991); J. J. Rehr, J. Mustre de Leon, S. I. Zabinsky, and R. C. Albers, J. Am. Chem. Soc. **113**, 5135 (1991).
[31] A. Filipponi, A. Di Cicco, and C. R. Natoli, Phys. Rev. B **52**, 15122 (1995).
[32] J. Cao, C. J. Bardeen, and K. R. Wilson, J. Chem. Phys. (submitted).
[33] L. Allen and J. Eberly, *Optical Resonance and Two-Level Atoms* (Dover, New York, 1987).
[34] C. J. Bardeen, J. Che, K. R. Wilson, V. V. Yakovlev, V. A. Apkarian, C. C. Martens, R. Zadoyan, B. Kohler, and M. Messina, J. Chem. Phys. **106**, 8486 (1997).
[35] G. Baym, *Lectures on Quantum Mechanics* (Addison-Wesley, New York, 1990).
[36] Our calculations were performed using FEFF 7.02 with the RGRID option set equal to 0.02. The standard setting of 0.05 was found to be too large to insure convergence for the inflated (relative to equilibrium) bond lengths found in our simulations.
[37] J. J. Boland, S. E. Crane, and J. D. Baldeschwieler, J. Chem. Phys. **77**, 142 (1982).
[38] E. A. Stern, Contemp. Phys. **18**, 289 (1978).
[39] L. V. Azaroff, Rev. Mod. Phys. **35**, 1012 (1963).
[40] The factors of 2 associated with the preceding formulas arise from the fact that a photoelectron must travel to and from the neighboring atom, thus traveling a distance twice the interatomic separation and interacting twice with the potential of the adsorbing atom. The lack of a factor of 2 in front of $\phi_j(k)$ is purely conventional.